J. Indian Chem. Soc.,
Vol. 97, No. 11b, November 2020, pp. 2407-2413

Benzene photo-mineralization in presence of metal ions in water containing suspended TiO_2 semiconductor

G. R. Dey*[a], C. Sharma[b], D. Sharma[b] and A. Ballal[c]

[a]Radiation and Photochemistry Division, Homi Bhabha National Institute, Bhabha Atomic Research Centre, Trombay, Mumbai-400 085, India

[b]Summer Project Trainees from Centre for Converging Technologies, University of Rajasthan, Jaipur-302 004, Rajasthan

[c]Molecular Biology Division, Homi Bhabha National Institute, Bhabha Atomic Research Centre, Trombay, Mumbai-400 085, India

E-mail: grdey@barc.gov.in

Manuscript received online 20 October 2020, revised and accepted 31 November 2020

Critical environmental pollutants of different types continue to challenge researchers to develop their mitigation methodologies. In this direction the semiconductor based photo-oxidation processes are good alternative for mineralization of organic pollutants. In this study we report our recent results on the mineralization of benzene (Bz) in aerated 0.1% (w/v) TiO_2 suspended aqueous systems in presence and absence of metal ions using 350 nm photo light. The metal ions such as Ag^+ and Au^{3+} are used separately under the study. The rate of Bz mineralization is significantly faster in Ag^+ or Au^{3+} containing TiO_2 systems in contrast to sole TiO_2 systems, which is due to the participation of metal ions and *in situ* generated various reduced metal ion intermediates including their nanoparticles in photo-degradation. The pre-generated nanoparticles of Ag and Au in TiO_2 systems also exhibit enhanced Bz mineralization separately. TEM studies reveal that (< 10 nm) silver nanoparticles (AgNP) in Ag^+ and (< 50 nm) gold nanoparticles (AuNP) in Au^{3+} containing TiO_2 systems are anchored on TiO_2 particles, which are probably responsible for faster Bz mineralization. Nevertheless, in metal ion containing TiO_2 systems, the nanoparticles generated *in situ* during photolysis show better photo-generated electron trapping properties. Under the study, Bz mineralization is faster in Au^{3+} containing systems as compared to Ag^+ containing systems which is due to larger AuNP particles generation on TiO_2 surfaces that exhibit better charge-carrier separation.

Keywords: TiO_2, mineralization, Au(III) ions, Ag(I) ions, benzene.

Introduction

Numerous chemicals generated in various anthropogenic activities discharged regularly into the environment, most of which are not only toxic but also non-biodegradable, thus not removed easily. This necessitates developing effectual methodology for degradation/mineralization of such materials and/or for their transformations to relatively less harmful materials. Photo-catalytic mineralization of organic pollutants is one of the easiest and affordable process in which semiconductors for instance TiO_2 is often used. In the present study we have carried out the photo-catalytic mineralization of benzene, a model pollutant using TiO_2 as suspension in water. Benzene, an eminent industrial organic chemical used as solvent, as a constituent in motor fuels, in extraction of oils from seeds and nuts, in manufacture of detergents, explosives, pharmaceuticals, and dyestuffs. It is found in emissions from burning coal and oil, motor vehicle exhaust, and evaporation from gasoline service stations. Trace level of Bz is also found in petroleum and coal. It is an offshoot of the incomplete combustion of many materials. These sources contribute to an elevated level of Bz in the ambient air[1] and subsequently to ground water. It is known to cause cancer[2] and considered as high level health hazard.

Moreover, the different forms of energy such as thermal, sonolysis, UV light, ionizing radiation and cold plasma (electrical) in presence and absence of catalysts and microorgan-

isms have been employed to oxidize a variety of organics[3–17]. Photo-catalytic reaction with non-toxic and economically easily available TiO_2 surfaces is renowned with the formation of charge carrier (e^- and h^+ (TiO_2^+) electron-hole pair)[18–20] on photo light irradiation only if energy of the incident photon is greater than the band gap energy of the semiconductor photo-catalyst. In presence of water/moisture the hole is transformed to $^\bullet OH$ through $h^+ + H_2O \rightarrow {}^\bullet OH + H^+ + TiO_2$ reaction ($^\bullet OH$ possesses strong oxidizing properties ($E° = 2.72$ V)[21]), whereas the counter negative ion (e^-) behaves as reducing species. Normally, oxygen or air available in the system has been utilized to scavenge photo-generated e^- by forming $O_2^{\bullet-}$ ($e^- + O_2 \rightarrow O_2^{\bullet-}$) and subsequently allowing the hole/h^+ for oxidation of available organics/pollutants. $O_2^{\bullet-}$ on the other hand behaves as a weak reductant ($E° = -0.33$ V)[22].

This work was explored further in the presence of metal ions (M^{n+}) such as Ag^+/Au^{3+} and/or silver nanoparticles (AgNP) and gold nanoparticles (AuNP) separately to ensure Bz mineralization, although the mineralization of organics in presence of metal doped TiO_2 is well known. The results presented depict that the significant contribution of metal nanoparticles and/or *in situ* generated various reduced species of metal ions on Bz mineralization with remarkable degradation kinetics.

Experimental

Materials and methods:

Titanium dioxide (TiO_2) (> 99% purity) from Aldrich, benzene (C_6H_6) of spectrograde from Spectrochem, India, silver perchlorate ($AgClO_4$) (99.9% purity) from Aldrich and gold(III) chloride as $HAuCl_4$ (99.9% purity) from Fluka, India were used as received. High purity water having conductivity < 0.05 μS cm^{-1} (obtained from 'Millipore Milli-Q' water system) was used for all solutions preparations.

A 40 ml capacity quartz cell was used for photo-irradiation with 350 nm light having photon flux 4×10^{15} photons cm^{-2} s^{-1} from a Rayonet photo-reactor. The amount of solution used in photolysis was 35 ml. The aerated (the air was purged for 10 min) aqueous solutions containing 0.1% (w/v) TiO_2 as suspension and 0.001–0.02 *M* Bz in presence and absence of M^{n+}/metal nanoparticles were photo-irradiated for different time with constant stirring at room temperature and normal atmospheric pressure. The total organic contents (TOC) were analyzed with TOC analyzer (Spectroquants Pharo 300 COD/TOC analyser). When required the membrane filter (Ultipor ®N_{66} ®Nylon 6.6 membrane 0.45 μm from PALL Life Sciences) was used for filtration of samples.

Materials characterization:

The filtrates of photo-irradiated samples were characterized with a spectrophotometer (JASCO V-650), whereas the characterization of residues on membrane filters was carried out with different analyzing techniques such as X-ray Diffractometer (XRD), Raman spectroscopy, Scanning Electron Microscopy (SEM) and Transmission Electron Microscopy (TEM). The XRD measurement was performed with Philips diffractometer (X'Pert PRO, PANalytical, Netherlands) using Ni filtered Cu K_α radiation of 1.54 Å (~8 keV energy). The XRD patterns obtained were later confirmed with the comparison of literature data and/or records within the library available in the software. Raman spectra were recorded at room temperature within the spectral range of 100 to 3000 cm^{-1} with a micro-Raman spectrometer (STR-300, SEKI Technotron, Japan). Additionally, the morphological images of the residue materials were obtained with JEOL JSM-T330 (for SEM) and Carl Zeiss LIBRA 120 kV (for TEM).

Results and discussion

Photolysis of Bz:

Aerated 0.01 *M* Bz in aqueous solution was photo-irradiated at 350 nm UV light up to 2 h. 5 ml of irradiated solutions were taken out at time intervals of 2, 5, 15, 30, 60 and 120 min and analyzed for TOC. The curve 1 in Fig. 1(a) represents the degradation trend of Bz obtained in this system. The mineralization or the conversion of Bz to CO_2 and H_2O was found to be negligible after the systematic comparison with TOC values obtained with samples of before and after photolysis. Hence, it is understood that the direct photolysis of Bz with 350 nm UV light did not lead to noticeable mineralization.

Photolysis of Bz in presence of TiO_2:

Similarly, aerated 0.01 *M* Bz in aqueous solution containing 0.1% (w/v) TiO_2 as suspension was photo-irradiated with 350 nm UV light. The irradiated solutions (5 ml) were taken out at different time intervals and TOC values obtained are shown in Fig. 1(a) curve 2. The photo-mineralization trend of Bz in presence of TiO_2 photo-catalyst was relatively faster as compared to the mineralization/degradation of Bz obtained

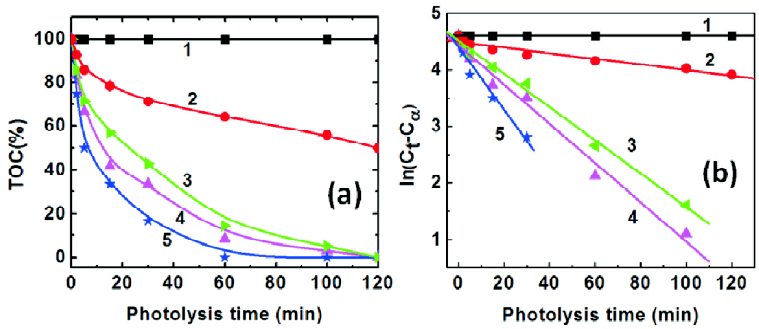

Fig. 1. (a) Photolytic degradation of 1: benzene (0.01 *M*); 2: Bz (0.01 *M*) with TiO_2 (0.1%) (w/v); 3: Bz (0.01 *M*) with TiO_2 (0.1%) (w/v) and Ag^+ (0.001 *M*); 4: Bz (0.01 *M*) with TiO_2 (0.1%) (w/v) and Ag^+ (0.005 *M*) and 5: Bz (0.01 *M*) with TiO_2 (0.1%) (w/v) and Ag^+ (0.02 *M*). (b) Photo-mineralization kinetics fittings obtained with all systems of Fig. 1(a).

in its absence. Approximately 50% of TOC was found in the photolytic solutions after 2 h of photo-irradiation. The mineralization rate evaluated from the plot of ln (C_t–C_∞) – ln C_∞ vs photolysis time [Fig. 1(b) fitting line 2) obtained using the data of curve '2' in Fig. 1(a) was 0.005 min^{-1} (Table 1) (where C_t and C_∞ represent TOC values respectively at time *t* and time ∞ (∞ represents the time where the TOC value becomes negligible)]. It is important to note that the samples were filtered to remove suspended TiO_2 particles using membrane filter and the UV-Vis spectra of filtrate samples were recorded within 200 to 300 nm wavelength region for analysis of left over Bz, as Bz exhibits absorption maximum (λ_{max}) at 253.6 nm. The spectra recorded (not shown) with pre- and post-photo-irradiated samples exhibit irregular behavior in spectral absorbance with respect to 253.6 nm absorption, which is due to the adsorption of a fraction of Bz on to TiO_2, therefore analyzing of Bz with absorption measurement at 253.6 nm was not adopted. Similar observation was also noticed during analyses of multiple samples containing identical concentrations of TiO_2 and Bz prior to carry out photo-irradiation experiments.

Photolysis of Bz in presence of TiO_2 and Ag^+:

Photo-catalytic work was explored further to verify the effect of metal ions such as silver ions (Ag^+) on Bz mineralization. To do so, aerated 0.01 *M* Bz in aqueous solutions containing 0.1% (w/v) TiO_2 as suspension in presence of different concentrations of Ag^+ (0.001, 0.005 and 0.02 *M*) were photo-irradiated separately. The irradiated 5 ml samples were taken out at different time intervals and TiO_2 therein was separated out through centrifuge and the supernatant solutions were analyzed using UV-Visible spectrophotometer. The UV-Vis spectra obtained (not shown) with the supernatant solutions of before and after 15 min photolysis reveal the formation of silver nanoparticles (AgNP) type materials. The absorbance in the visible region increases with Ag^+ concentrations. The change in colors of solutions and residues on membrane filters from white due to TiO_2 to dark yellow (not shown) in Ag^+ containing systems designated the formation of AgNP upon photo-irradiation. It was also noticed that the intensity of color of solutions and residues changes with photo-irradiation time.

Characterization of materials:

The XRD patterns of residue materials on membrane filters obtained before and after photo-irradiation of aerated Bz (0.01 *M*) – Ag^+ (0.02 *M*) – TiO_2 (0.1% w/v) samples in water are shown in Fig. 2(a). The XRD pattern of TiO_2 (peaks at 2θ = 25° and 48°) obtained are quite similar to that reported for anatase TiO_2[23,24] and remained unaffected in Bz-TiO_2 systems containing Ag^+. However, with 60 and 120 min photo-irradiated Bz (0.01 *M*) – Ag^+ (0.02 *M*) – TiO_2 (0.1% w/v) samples, a small change in peaks intensities at 2θ = 44.5° (Fig. 2(a), pattern 3) was noticed, which is probably due to AgNP formation. Similarly, the Raman scattering measurement records with the residues on membrane filters are shown in Fig. 2(b). Three distinct peaks at 637, 514 and 396 cm^{-1} were observed in presence of TiO_2 (Fig. (2b), spectrum '1'), which are identical to earlier reports[17,25]. The presence of Bz and Ag^+ (before photolysis) did not show any considerable change in the Raman spectral properties of TiO_2 (Fig. (2b), spectrum '2') except minute peak intensity reduction. Moreover, in 60 min photo-irradiated samples the peaks de-shaping (broadening, and shifting to 634, 517 and 398 cm^{-1})

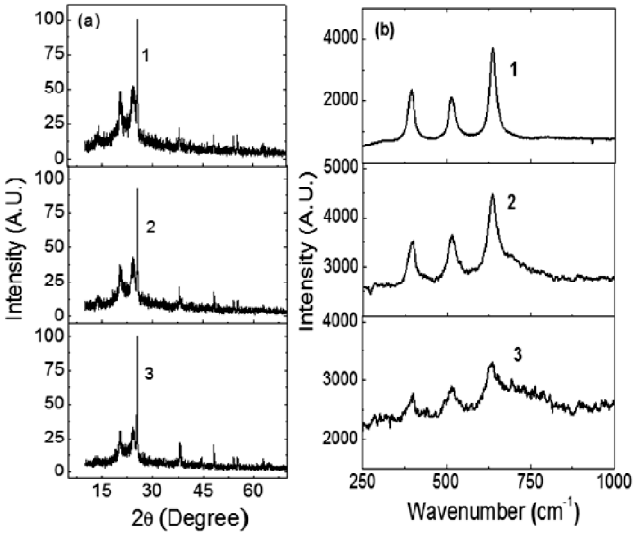

Fig. 2. (a) XRD patterns and (b) Raman spectra observed with residues of different samples on membrane filter: 1: TiO_2 (0.1%) (w/v); 2: TiO_2 (0.1%) (w/v), Bz (0.01 *M*) and Ag^+ (0.02 *M*); 3: after 60 min photolysis of TiO_2 (0.1%) (w/v), Bz (0.01 *M*) and Ag^+ (0.02 *M*).

within 1000 cm^{-1} were observed, which is due to the active interaction between TiO_2 and AgNP (produced in photo-irradiation), (Fig. 2(b), spectrum 3) that changed the vibration and structural properties of TiO_2 as explained previously with AuNP interaction with TiO_2[17,25].

The SEM images obtained with TiO_2, TiO_2 with Bz and Ag^+, and 30 and 60 min photo-irradiated TiO_2 with Bz and Ag^+ samples did not show any considerable change except slight coagulation in the photo-irradiated samples, hence not shown separately. Moreover, the morphological change was distinctly visible in TEM images as shown in Fig. 3(a) and (b). The image b in Fig. 3 exhibited AgNP incorporated on TiO_2 surfaces (probably Ag as doped state) that perhaps revealed high mineralization efficiency in contrast to solitary TiO_2 (Fig. 3a). The size of small grain like structure of Ag on TiO_2 as shown in Fig. 3(b) was < 10 nm. It is noteworthy to include at this point that the TEM images of AgNPs, which were generated either *in situ* during mineralization or prior to Bz photo-mineralization experiments found were identical.

Benzene mineralization trends observed in Ag^+ containing TiO_2 systems were much faster as compared to lone TiO_2 systems (curves 3-5 in Fig. 1(a)). The mineralization rates in presence of different concentrations of Ag^+ evaluated similarly as discussed above and the values are listed in Table 1. The rates listed in Table 1 were found to be Ag^+ concentration dependent and found highest with 0.02 *M* Ag^+.

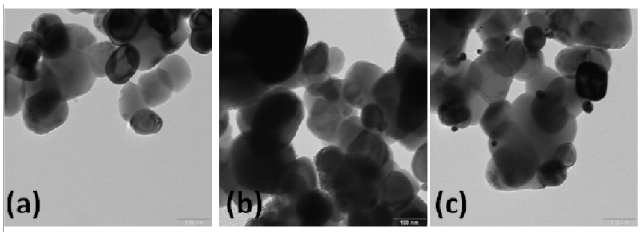

Fig. 3. TEM images (a): TiO_2; (b): Ag-TiO_2 and (c): Au-TiO_2 samples.

Table 1. The Bz mineralization rates evaluated in presence of various concentrations of Ag^+ in TiO_2 containing aqueous systems

[Bz]	[TiO_2]	[Ag^+]	Rate
M	w/v%	*M*	(min^{-1})
0.01	0.1	0	0.00506
0.01	0.1	0.001	0.0294
0.01	0.1	0.005	0.0347
0.01	0.1	0.02	0.0555

Photolysis of Bz in presence of TiO_2 and AgNP:

Benzene mineralization work was explored further to verify the impact of AgNP, which supposed to be a bye product in photo-catalytic experiments in TiO_2 systems containing Ag^+ (discussed above). To ensure this, AgNPs were generated prior to Bz photo-mineralization experiments by carrying out photolysis of aerated 0.1% (w/v) TiO_2 with three different Ag^+ (0.001 *M*, 0.005 *M* and 0.02 *M*) concentrations for 2 h separately using 350 nm photo light. Similar mineralization experiments were carried out after mixing appropriate concentration of Bz (0.01 *M*) with previously generated different concentrations of AgNPs in TiO_2 systems separately and the TOC changes curves obtained are shown in Fig. 4(a). For evaluation purpose, Bz mineralization experiment was carried out with an identical sample (0.001 *M* AgNP and Bz (0.01 *M*)) at room temperature but without photolysis at 350 nm light. The mineralization curve (curve 1 in Fig. 4(a)) generated without photo-irradiation was found to be very slow as compared to photo-irradiation samples. To examine the combined effect of AgNP and Ag^+, a previously prepared 0.001 *M* AgNP was mixed with 0.001 *M* Ag^+ and checked Bz (0.01 *M*) mineralization kinetics by carrying out similar photolysis

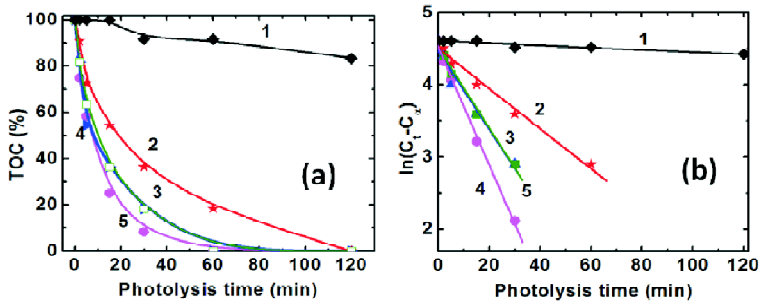

Fig. 4. (a) Photo-mineralization of Bz in 1: Bz (0.01 *M*) with TiO_2 (0.1%) (w/v) and AgNP (0.001 *M*) without photolysis; 2: Bz (0.01 *M*) with TiO_2 (0.1%) (w/v) and AgNP (0.001 *M*); 3: Bz (0.01 *M*) with TiO_2 (0.1%) (w/v) and AgNP (0.005 *M*); 4: benzene (0.01 *M*) with TiO_2 (0.1%) (w/v) and AgNP (0.02 *M*) and 5: Bz (0.01 *M*) with TiO_2 (0.1%) (w/v), AgNP (0.001 *M*) and Ag^+ (0.001 *M*) systems. (b) Mineralization kinetics of all systems of Fig. 4(a).

experiments. The mineralization curve (curve 5 in Fig. 4(a)) was quite similar to Bz degradation kinetics observed with AgNP (0.005 *M*) revealing Ag^+ or *in situ* higher concentration of AgNP contribute significantly on Bz mineralization. On comparison it was found that the mineralization of Bz was faster in case of AgNP, and the evaluated kinetics values are listed in Table 2.

Table 2. The list of mineralization rates evaluated in systems containing previously generated AgNP in presence and absence of Ag^+

[Bz] *M*	[TiO_2] (w/v)%	[Ag^+] *M*	[AgNP] *M*	Rate (min^{-1})
0.01	0.1	0	0.001*	0.0016
0.01	0.1	0	0.001	0.028
0.01	0.1	0	0.005	0.054
0.01	0.1	0	0.02	0.081
0.01	0.1	0.001	0.001	0.055

*Represents no photolysis.

Photolysis of Bz in presence of TiO_2 and Au^{3+}:

Similarly, photo-irradiation of aerated 0.01 *M* Bz in aqueous solutions containing 0.1% (w/v) TiO_2 as suspension in presence of two different Au^{3+} concentrations (0.0001 and 0.001 *M*) were carried out separately using 350 nm photo light. The mineralization curves obtained with respect to TOC values at different photolysis time are shown in Fig. 5(a). The curves 2 and 5 exhibit the faster Bz mineralization as compared to only TiO_2 system (curve 2 in Fig. 1(a)). The mineralization rates evaluated are listed in Table 3. Fig. 5(a) and (b) and Table 3 reveal that the presence of either 0.001 *M* Au^{3+} or previously generated AuNP with 0.001 *M* Au^{3+}, the mineralization rates observed were identical showing the significance of *in situ* generated AuNP in Bz mineralization in Au^{3+} containing systems. Material characterization (TEM

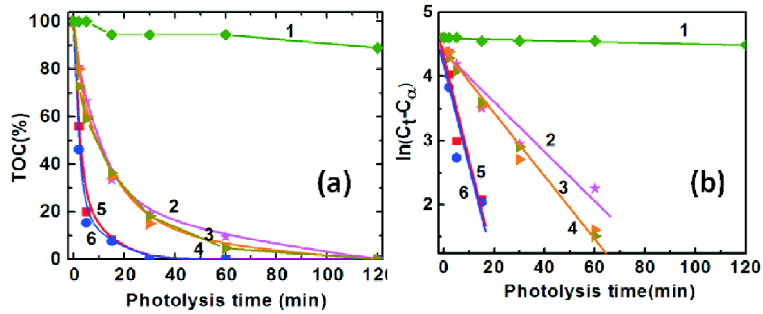

Fig. 5. (a) Photo-mineralization of Bz in 1: Bz (0.01 *M*) with AuNP (0.001 *M*) without photolysis; 2: Bz (0.01 *M*) with TiO_2 (0.1%) (w/v) and Au^{3+} (0.0001 *M*); 3: Bz (0.01 *M*) with TiO_2 (0.1%) (w/v) and AuNP (0.0001 *M*); 4: Bz (0.01 *M*) with TiO_2 (0.1%) (w/v), AuNP (0.0001 *M*) and Au^{3+} (5×10^{-5} *M*); 5: Bz (0.01 *M*) with TiO_2 (0.1%) (w/v) and Au^{3+} (0.001 *M*) and 6: Bz (0.01 *M*) with TiO_2 (0.1%) (w/v) and AuNP (0.001 *M*) containing systems. (b) Mineralization kinetics of all systems presented in Fig. 5(a).

Table 3. List of the mineralization rates evaluated in various Au^{3+} and/or AuNP containing systems

[Bz]	[TiO_2]	[Au^{3+}]	[AuNP]	Rate
M	(w/v)%	*M*	*M*	(min^{-1})
0.01	0.1	0	0.001*	0.0009
0.01	0.1	0.0001	0	0.0386
0.01	0.1	0	0.0001	0.0492
0.01	0.1	0.00005	0.0001	0.0491
0.01	0.1	0.001	0	0.1591
0.01	0.1	0	0.001	0.1560

*Represents no photolysis.

image, Fig. 3(c)) reveals that Au-TiO_2 generated *in situ* possesses ~50 nm sized gold nanoparticles (AuNP) anchored over TiO_2 particles is possibly responsible for faster Bz mineralization.

It is understood from the material characterization studies that the difference in morphological change as discussed above lead to the formation of *in situ* AgNP/AuNP and/or Ag/Au-doped TiO_2. Even in aerated metal ions (M^{n+}) containing TiO_2 systems, M^{n+} (Ag^+/Au^{3+}) ions have shown better electron scavenging properties than oxygen resulting in enhanced Bz mineralization. Under the study, the various concentrations of M^{n+} exhibited different mineralization kinetics revealing that the mineralization in presence of air was M^{n+} concentration dependent. Oxygen served both as scavenger of photo-generated electron and provider of O_2 for the transformation of pollutant (Bz) to CO_2 and H_2O. The important part under the study was the formation of metal nanoparticles (MNP) following the reduction reactions pathway even in presence of air (~20% O_2 equivalent to 0.24 mM). Normally, the generation of MNP takes place with the initial metal atom (or reduced metal ions) formation through e^- – M^{n+} reduction reactions. Later it followed aggregation with solute metal ions through multi steps nucleation reactions[26] and finally leads to the formation of metal nanoparticles. It is noteworthy to include that the e^- reactions with Ag^+/Au^{3+} ions in aqueous solutions were diffusion controlled[27] and MNP were generated instantly perhaps on the surface of TiO_2 competing e^- – O_2 scavenging reaction. Moreover, as reported earlier, in the gold doped/caped TiO_2 (Au/TiO_2) systems the metal nanoparticles have been considered as an electron sink/trapper[28], where the electrons in the conduction band are capable to migrate towards the Au surface, thereby preventing the recombination of e^- and h^+ charge carrier. Under the study this separation was more in Au^{3+}/AuNP systems than Ag^+/AgNP systems as anchored/caped Au in AuNP possesses higher diameter (~50 nm) in TEM image. As a result more e^- and h^+ were utilized in respective reduction and oxidation processes. Thus h^+ was favoring faster Bz mineralization in Au^{3+} or AuNP containing TiO_2 systems. On the other hand, as mentioned above, the oxygen available produces superoxide radical anion ($O_2^{\bullet-}$) after reaction with a fraction of e^-, and subsequently converted into $^\bullet OH$ via $HO_2^\bullet/H_2O_2$, resulting further enhancement in Bz mineralization. Moreover, the major part of e^- was involved in metal nanoparticles formation showing dual nature of metal ions (formation of MNP as well as scavenger of photo-generated e^-). Nevertheless, in M^{n+} containing systems, after formation of MNP (as soon as color appears) the systems behave both as metal doped as well as metal ions containing systems, wherein both M^{n+}, reduced M^{n+} species and MNP play significant role in Bz mineralization. This happens only when the photolysis is kept on, because after photolysis (photo light off condition) the colors of nanoparticles remain steady, indicating the negligible contribution of Bz mineralization through thermal reaction. It is noteworthy to include that the active role of various intermediates starting from reduced metal ions/metal atom to oligomers/small aggregates including metal nanoparticles were important in pollutants photodegradation. In TiO_2 based systems, the phenol/phenolic compounds has also been reported as an intermediate product from Bz and benzene derivatives[12,29]. The overall photo-catalytic reaction mechanism for higher mineralization kinetics in metal ion containing systems is summarized in Scheme 1.

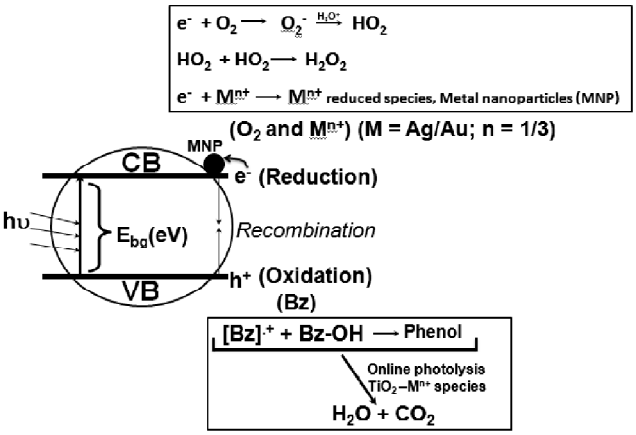

Scheme 1. Redox reactions during photolysis of Bz with TiO_2 in metal ions containing systems.

Conclusions

Photocatalytic mineralization of Bz has been successfully demonstrated in presence of Ag^+ and Au^{3+} separately in aerated TiO_2 systems. Bz mineralization rate was faster in presence of metal ions and MNP in TiO_2 containing systems. In both the systems Bz degraded much faster than in sole TiO_2 containing systems. The mineralization kinetics in presence of air was dependent on M^{n+}/MNP concentration. The strong interaction of MNP with TiO_2 in Raman shifting reveals the attachment of metal nanoparticles with the semiconductor. Furthermore, in TEM studies, ~50 nm AuNP and ~10 nm AgNP were anchored on TiO_2 surfaces, which are possibly enhancing e^- - h^+ separation hindering charge-carrier recombination. Larger size AuNP nanoparticles favoured more charge carrier separation resulting faster Bz mineralization than smaller sized AgNP. Furthermore, the anchored AgNP/AuNP TiO_2 possesses optical absorption in the visible region, projecting a better choice for solar light utilization in mineralization of organic pollutants. The above findings not only contribute in updating the Bz mineralization technique, but this methodology can evolve as a suitable technique for their utilization in pollution mitigation.

Acknowledgements

This research was carried out under the plan project no: XII-N-R&D-02.1. CS and DS thank Centre for Converging Technologies, University of Rajasthan, and BARC authorities for approving their summer intern ships. Authors thank Bhabha Atomic Research Centre and the Department of Atomic Energy, Government of India for funds and Dr. A. Guleria from RPCD for Raman spectrum measurements.

References

1. L. A. Wallace, *Environ. Health Perspect*, 1989, **82**, 165.
2. Cause cancer http://www.cancer.org/cancer/cancercauses/othercarcinogens/intheworkplace/benzene accessed 27 Sept 2016.
3. J. Zhong, J. Wang, L. Tao, M. Gong, L. Zhimin and Y. Chen, *J. Hazard. Mater.,* 2007, **139**, 323.
4. J. D. Coates, R. Chakraborty, J. G. Lack, S. O'Connor, K. A. Cole, K. S. Bender and L. A. Achenbach, *Nature*, 2001, **411**, 1039.
5. H. Park and W. Choi, *Catal. Today,* 2005, **101**, 291.
6. X.-M. Pan, M. N. Schuchmann and von C. Sonntag, *J. Chem. Soc., Parkin Trans. 2*, 1993, 289.
7. D. Ascenzi, P. Franceschi, G. Guella and P. Tosi, *J. Phys. Chem. A,* 2006, **110**, 7841.
8. Z. Ye, Y. Zhang, P. Li, L. Yang, R. Zhang and H. Hou, *J. Hazard. Mater*., 2008, **156**, 356.
9. E. Hisahiro and O. Atsushi, *J. Hazard. Mater.,* 2009, **164**, 1236.
10. T. N. Das and G. R. Dey, *J. Hazard Mater.*, 2013, **248-249**, 469.
11. G. R. Dey, A. Sharma, K. K. Pushpa and T. N. Das, *J. Hazard. Mater*., 2010, **178**, 693.
12. G. R. Dey, *Res. Chem. Intermed.,* 2009, **35**, 573.
13. G. R. Dey and P. Singh, *J. Appl. Sol. Chem. Model,* 2017, **6**, 28.
14. P. Singh, A. Borthakur, N. Srivastava, R. Singh, D. Tiwary and P. K. Mishra, *Pollution*, 2016, **2**, 199.
15. H. Zhuang, Q. Gu, J. Long, H. Lin, H. Lin and X. Wang, *RSC Adv*., 2014, **4**, 34315.
16. E. A. Edwards and D. Grbic-Galic, *Appl. Environ. Microbio.,* 1992, **58**, 2663.
17. H. Keller, S. Kleinsteuber and C. Vogt, *Microb. Ecol.,* 2018, **75**, 941.
18. M. R. Hoffmann, S. T. Martin, W. Choi and D. W. Bahnemann, *Chem. Rev.,* 1995, **95**, 69.
19. D. W. Bahnemann, in: "Photochemical conversion and storage of solar energy", eds. E. Pelizzetti and M. Schiavello, Kluwer, Dordrecht, 1991, p. 251.
20. G. R. Dey, "Transformation of carbon dioxide to useable products through free radical induced reactions", in: 'Green carbon dioxide: Advances in CO_2 utilization', eds. G. Centi and S. Perathoner, John Wiley, USA, 2014, pp. 25-50.
21. J. W. T. Spinks and R. J. Woods, in: "An introduction to radiation chemistry", Wiley, New York, 1990.
22. B. H. J. Bieski, D. E. Cabelli, R. L. Arudi and A. B. Ross, *J. Phys. Chem. Ref. Data*, 1985, **14**, 1041.
23. D. Belapurkar, V. S. Kamble and G. R. Dey, *Mater. Chem. Phys*., 2010, **123**, 801.
24. G. R. Dey, *J. Appl. Sol. Chem. Model,* 2015, **4**, 63.
25. H. C. Choi, Y. M. Jung and S. B. Kim, *Vib. Spec*., 2005, **37**, 33.
26. J. Belloni, *Catal. Today*, 2006, **113**, 141.
27. G. V. Buxton, C. L. Greenstock, W. P. Helman and A. B. Ross, *J. Phys. Chem. Ref. Data*, 1988, **17**, 513.
28. V. Subramanian, E. E. Wolf and P. V. Kamat, *J. Am. Chem. Soc*., 2004, **126**, 4943.
29. P. V. Kamat, *Chem. Rev*., 1993, **93**, 267.